Volume 1 | Number 1 | Jan 2013 | Pages 1–100

Journal of
Materials Chemistry C

Materials for optical and electronic devices
www.rsc.org/materialsC

ROYAL SOCIETY
OF CHEMISTRY

ROYAL SOCIETY
OF CHEMISTRY

www.rsc.org/materialsC

Naturally self-assembled nickel nanolattice

Jaiveer Singh,[a] Netram Kaurav,[b] Niranjan Prasad Lalla[c] and Gunadhor Singh Okram[*d]

This is the report on the critical nature of nanolattice formability of different particle size (~ 4 – 10 nm) of monodispersed nickel nanoparticles. They exhibit strikingly hexagonal close-packed (hcp) nanolattices without extra forces, whenever trioctylphosphine (TOP) is (one of) the surfactant(s). This clearly establishes the unique role of nanolattice formability of TOP. The c/a ratios are interestingly identical to those of atomic lattices. An attempt has also been made to explain them based on the balanced attractive and repulsive forces of the surfactant-generated cation-anion pairs on the surface of the nanoparticles. The present findings therefore will provide a far-reaching vista to fabrication of varieties of natural nanolattices and their understanding on applications in a new paradigm.

Introduction

The properties of nanoparticle lattices (nanolattices) are distinct from those of individual nanoparticle or bulk counterparts. They are highly attractive for future advanced applications[1-5] but have so far been enabled artificially using extra forces.[6-11] For example, tributylphosphine has been used for nickel nanolattice[6] formation similar to those of gold[12] and iron oxide.[13] Assembly of nanoparticles of two different materials into a binary nanolattice of varieties of materials (to enable opposite electrical charges on nanoparticles to impart a specific affinity of one type of particle)[2,11] or a nanolattice of oppositely charged nanoparticles[14] has been studied. However, such impressions of the compulsory use of an external agent seems to be due to the poor knowledge of surfactants in general (or specifically TOP) since such so-called non-ionic surfactant is *usually ionic* due to the possible formation of cation-anion pairs from dissociated surfactant molecules or impurities.[15,16] This will then favor mimicking the naturally balanced electrostatic cohesive and repulsive energies of electrons and nuclei found in atomic lattices[17,18] without external forces and hence natural formability of nanolattice. This possibility, if proven, strongly suggests the paramount versatility of TOP as one of the surfactants in the preparation of nanoparticles as it also most probably enables monondispersity.[6,19-25] This hypothesis also supports the probable unproven signature of CdSe nanolattice formation due to the presence of TOP as one of the surfactants.[24] To critically test for natural nanolattice formability, we chose the case for nickel nanoparticles prepared from nickel acetylacetonate by fixing the content of one of the favorite surfactants or stabilizers among researchers (viz., oleylamine (OAm)[6,19], TOP[6,19-25] and triphenylphosphine (TPP)[6]) while varying one of them or using only a single surfactant independently. Thus, we demonstrate (i) the formation of strikingly natural hcp nanolattices of nickel when no extra forces are used with the nanoparticles prepared as usual, whenever TOP is (one of) the surfactant(s), (ii) the unqiue role of nanolattice formabilty of TOP and (iii) the naolattice parameters, calculated analytically, to have c/a ratios identical to those of atomic lattices. These have been established concretely using, among others, small angle X-ray scattering (SAXS), transmission electron microscopy (TEM), zeta potential, Fourier-transformed infra-red (FTIR) and X-ray photoelectron spectrocopoy (XPS) techniques.

Experimental

Synthesis of monodispersed nickel nanoparticles

Thermal decomposition method as in references[6,19] was used to synthesize the nanoparticles. Typically, 1 ml (i.e. 2.24mM) of preheated (215 °C) TOP (90% Aldrich) was added in the already degassed (at 100 °C for 30 min) solution of 1.02 g Ni(acac)$_2$ (95% Aldrich) and 8 ml OAm (70% Aldrich). The resulting solution was further heated at 220 °C for 2h under argon atmosphere. This gave rise to black precipitate due to formation of nickel nanoparticles. Solution was then cooled to 27 °C, and centrifuged by adding ethanol (99.9% Jiangsu Huaxi) to extract and wash the nanoparticles. Washing was done four times. Similar procedures were followed for 3 ml, 5 ml, 8 ml and 10 ml of TOP at fixed (8 ml) OAm; trioctylephosphine in X ml will denote the samples here. In addition to these samples, several other samples were prepared for (a) varying OAm with fixed TOP, (b) varying TPP (99% Aldrich) with fixed OAm and (c) separately for each of these surfactants. The particles were dried at 60 °C and used directly for characterizations.

Synchrotron SAXS and XRD measurements

Synchrotron radiation (1.089Å) X-ray diffraction (XRD) data was collected at BL-18B (Indian beamline), Photon Factory, Tsukuba, Japan with a beam current of 401 mA in the angle ranges 0.2-2° and 9-30° for angular step of 0.025° with a point detector (Cyberstar) on powdered samples and glass drop-casted thin films. The thin films were made after thorough sonication of the nickel nanoparticles dispersed in ethanol. The incident X-ray angle for small angle X-ray scattering (SAXS) measurements was 0.15-0.25°.

Laboratory X-ray Diffraction

The Bruker D8 Advance X-ray diffractometer with Cu Kα radiation (0.154 nm) in the angle range 20-90° was used for laboratory method of XRD measurements of the samples in powder form; the X-rays were detected using a fast counting detector based on silicon strip technology (Bruker LynxEye detector).

Laboratory high resolution SAXS

High resolution laboratory SAXS measurements on glass drop-casted thin films were done with Cu Kα radiation in the angle range 0.2-10° with a step size of 0.02°; the incident X-ray angle was normally fixed at 0.5° unless it is specified.

Transmission electron microscopy (TEM)

Nanoparticle images and selected area electron diffraction (SAED) were recorded using transmission electron microscopy

(TECHNAI-20-G^2) by drop-casting the well-sonicated solution of a few milligrams of nanoparticles dispersed in about 5 ml ethanol on carbon-coated TEM grids.

Zeta potential measurements

Zeta potential measurements using a Zetasizer (Malvern ZS-90) were done after thorough sonication of the nanoparticles dispersed in different dispersants. Approximately 8 mg nanoparticles were dispersed in 15 ml of the dispersant, say ethanol, hexane and TOP for a typical run. The number of runs made was in the range 50-100.

Fourier-transformed Infra-Red (FTIR) absorption measure ments

A few micrograms of the nanoparticles of each sample were added to a fixed quantity of pure KBr and ground it thoroughly. Then, a pellet of the uniform mixture was made for each sample. Two or three drops of each of TOP, OAm and ethanol were added to similar size pellets of pure KBr. FTIR spectrum of a pure KBr pellet was subtracted from the FTIR data of each sample to obtain the corresponding FTIRs of the samples.

X-ray photoelectron spectroscopy (XPS) measurements

The XPS measurements were performed using a Phoibos 1000 electron energy analyzer from Specs GmbH, Germany with 50 eV pass energy. Al-Kα laboratory x-ray source operated at 100 watts provided photons of energy 1486.6 eV. The required correction for the XPS spectra was done. The experimental error was below $\pm$ 0.1 eV and the spectrometer resolution was better than 1 eV. These data were used for identifying the compositions of the nanoparticles.

Results and discussion

Study of nanolattice formation through SAXS, XRD and TEM

The small angle X-ray scattering is a powerful tool to identify the nanolattice structures.[7] These data for the nickel nanoparticles of different particle sizes ($\sim$ 4 – 10 nm) prepared in OAm and TOP, without any other *extra* surfactant, reagents or external forces are shown in Figure 1. Several low angle peaks clearly observed in the SAXS data are assigned to the lattice planes formed by the monodispersed nanoparticles. Since no extra forces are used to prepare them, they indicate the natural formation of nanolattices that are distinct from wide angle X-ray diffraction (XRD) as the latter is due to the atomic face-centered cubic (fcc) lattice (Figure 2 and S1 in the Electronic Supplementary Information (ESI)). (Samples were found to be stable according to our XRD data since they do not show peaks related to the oxide even after several months contrary to that reported [6] of complete oxidation within 24 h.) The selected area electron diffraction patterns of the nanoparticles for the electron beam perpendicular (Figure 1a, bottom left inset) and parallel to the plane of TEM grid plane (Figure 1a, bottom middle inset) for 10 ml sample reveal *local* self-assembly of hcp lattice of nanoparticles in two-dimensions. Figure 1a, bottom right inset shows an expanded TEM image of hexagonal arrangement of seven nanoparticles of nearly spherical shapes. Figure 3 shows the typical TEM images of four samples of monodispersed nanoparticles. The statistical distribution plots of particle sizes (Figure 3, upper insets) indicate their monodispersed nature and respective average size. The selected area electron diffraction of the lattice (Figure 2, right panel, lower

insets) confirms the fcc structure of the atomic lattice seen from XRD (Figure 2).

To ensure that the peaks in Figure 1 b, c and d are due to self-assembly of bulk 3D hcp structure of nanoparticles, *analytical calculations*[26] were made using these peaks. For this, $\sin^2\theta$ values were determined from

$$\sin^2\theta = A(h^2 + hk + k^2) + Cl^2, \qquad (1)$$

where A=$\lambda^2/3a^2$, C=$\lambda^2/4c^2$, λ is wavelength of the X-ray and other parameters have their usual meanings. Permissible values of (h^2+hk+k^2) being 1, 3, 4, 7, 9, etc for hcp structure, the observed $\sin^2\theta$ values were divided by 1, 3, 4, etc. These numbers were examined to find out that any of the quotients (nearly) match the observed $\sin^2\theta$ values and hence the tentative value of A was determined. The correspondingly matched values of (hk0) were chosen as the expected (hk0) values. Using these (hk0), and A(h^2+hk+k^2) values, value of C is determined from equation (1) such that Cl^2 is in the ratio of 1, 4, 9, 16, etc. This procedure readily enables to identify the peaks in the pattern systematically. Final check was done by a comparison of observed and calculated $\sin^2\theta$ values.
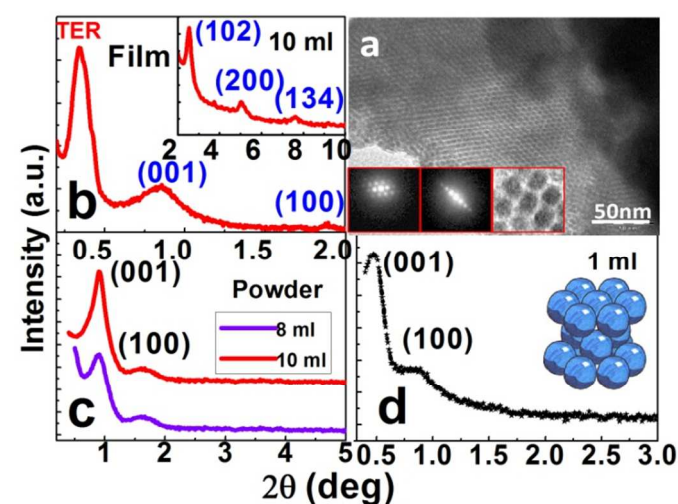

Fig. 1 Transmission electron microscopy (TEM) images and SAXS patterns of Ni nanoparticles. (a) Representative TEM image of 10ml sample nanoparticles. Inset: SAED of hexagonally arranged self-assembled Ni nanolattice when the electron beam is perpendicular (left) and parallel (middle) to the plane of copper grid, and magnified portion of seven (hexagonally arranged) nanoparticles (right). (b) SAXS of glass-drop-casted film of 10 ml sample with higher angle in inset. The analytically calculated (hkl) values for hcp phase are given; total external reflection (TER) is due to glass substrate. (c) Powder SAXS for 10 ml and 8 ml Ni bulk nanoparticle samples. (d) Powder SAXS of 1 ml Ni bulk nanoparticle sample. Inset: an illustration of hexagonal closed-packed unit cell representing the nanoparticle unit cell.
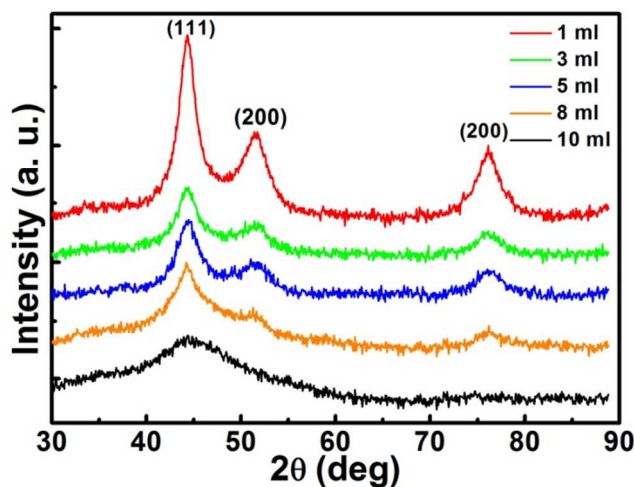
Fig. 2 X-ray diffraction data of nickel nanoparticles prepared for 1 ml, 3 ml, 5 ml, 8 ml and 10 ml trioctylphosphine content for fixed nickel acetylacetonate and OAm concentrations. Diffraction angle was converted to 1.5406 Å wavelength equivalent of copper to compare the laboratory XRD results.
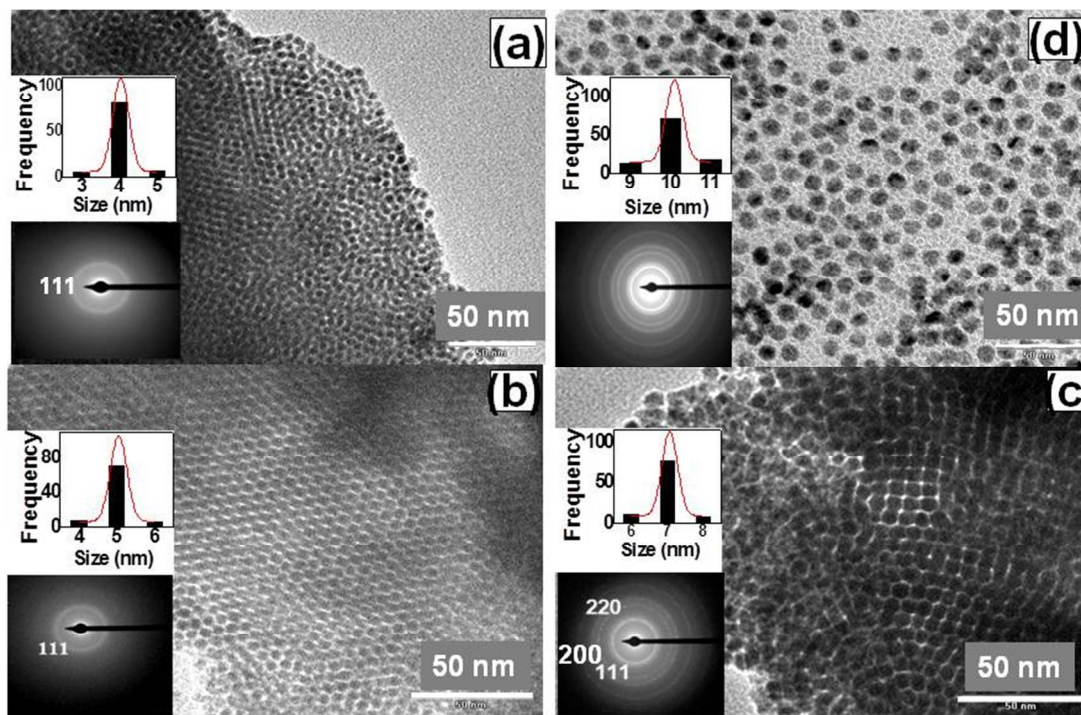

Fig. 3 Transmission electron microscopy images of (a) 10 ml, (b) 8 ml, (c) 3 ml and (d) 1 ml sample nanoparticles. Scales indicated are 50 nm. Insets: The statistical distribution plots of particle sizes and their fits (upper), and selected area electron diffraction of the atomic lattice (lower).

The SAXS peaks of the 10ml sample can thus be systematically correlated with (hkl) values of bulk 3D hcp nanolattice (Figure 1b) that has the nanolattice parameters, a = 3.812(7) nm, c = 7.131(50) nm and c/a = 1.87. The peak near $2\theta = 0.36°$ was identified as the total external reflection from glass substrate (Figure S2 in the ESI). In contrast, our attempt to find out the peak positions for their probable fcc nanolattice using the average particle size of 4.0 nm as lattice spacing were always different from those observed. This proves that the observed SAXS peaks are due to bulk 3D hcp nanolattice, not due to fcc nanolattice. The peaks of the other samples were also identified as hcp nanolattice. The 10 ml and 8 ml samples in powder forms show hexagonal structure (Figure 1c) with a, c and c/a of 4.390(5) nm & 4.40(2) nm, 7.31(3) nm & 7.45(4) nm and 1.67 & 1.69, respectively. For 10 ml powder sample, the

nanolattice parameters are slightly bigger than those of thin film. The nanolattice parameters of 1 ml powder sample (Figure 1 d) are a = 8.09(6) nm, c = 13.280(5) nm with c/a = 1.64. These natural bulk hcp nanolattices even in powder form are striking. They imply that such nanolattices should prevail even in compacted pellets as well as in refs. [27,28], similar to sample powder of atomic lattices.[17,18,26] The ratio c/a = 1.64 - 1.87 found is similar to atomic lattices indicating their close analogy. Notably, value of the nanolattice parameter a is smaller in some of nanolattices than the average particle size. This is explained on the basis of adjustable cappant thickness.[8,9]

In order to comprehensively establish the genuine origin of formation of the natural nanolattice is due to the use of TOP or any other surfactant, we have recorded the SAXS patterns (Figure S3 in the ESI) of the several other samples prepared for (i) varying OAm with fixed TOP, (ii) varying TPP with fixed OAm and (iii) separately for each of these surfactants. Remarkably, the SAXS peaks associated with the nanolattice formation is naturally observed whenever TOP only or in combination of it with other surfactants are used for the sample preparations, but not with TPP and OAm separately. The nanolattice observed is therefore ascribed to the TOP that in turn also is expected to prove the vestiges of nanolattices seen in ZnS and CdSe[24] and nickel[6] nanoparticles as due to the TOP. The natural cohesive energy of the nanolattice is attributed to the dissociated molecules or impurities of TOP.[15,16] The large clusters of these nanolattices for average particle sizes of 4 nm, 5.1 nm, 7.1 nm and 10.1 nm can be clearly seen from TEM images in bigger scales (Figure S4 in ESI).

Zeta potential properties

To ascertain the stability of these nanolattices and prove its formability, we have carried out their zeta potential (ζ) measurements. We note that ethanol might assume crucial if the

small while those of -19 to -38 mV in TOP are relatively large. This indicates that influence of ethanol to TOP ligands on the electric double layers of the particles is marginal while that of TOP dispersant to its bound counterparts on the surface of nanoparticles is significantly large that increases with its number of ligands. The lowering of zeta potential with increase in TOP is explained based on the enhanced agglomeration of the nanoparticles into nanolattice thereby leading to reduced number of uncompensated negative charges and hence reduced zeta potential values. Another possibility is the less acetylacetonate (acac⁻) ligand/ ion compensation with TOP at lower concentration of TOP than those at higher concentrations, thereby controlling the negative charge neutrality if formation of a complex of P with acac ligands is assumed; this is further discussed in FTIR and XPS studies. The TOP concentration normally leads to reduction in particle size (Figure 4, Size curve), since efficiency in rapid and short nucleation phase and slow growth kinetics would increase with TOP concentration increases.[29] The situation for hexane is however very random (Table 1). The small values of ζ indicate the weak ionic nature of surfactants that in turn seem to confirm the formation of aggregates i.e. nanolattice.[16] The weak ionic nature combined with high values of conductivity and mobility of the nanoparticles in ethanol, 0.392 - 10.2 µS/cm and -0.1768 - 0.1148 µmcm/Vs, respectively (Table 1) would indicate that these non-ionic surfactants are quite ionic. They are attributed to cation-anion pairs formed from the minute contaminants or dissociation of TOP molecules.[15,16] This leads to the formation of nanolattice, well in agreement with the Bjerrum radius[16] (~28 nm) that is much larger than the size of present nanoparticles (4 – 10 nm).

formation of nanolattice was also related to it as the nanoparticles were washed with or dispersed in it. The ζ data for samples prepared in TOP and OAm together measured in ethanol, hexane and TOP separately are represented in Figure 4. These ζ values in the range of -1 to 1.5 mV in ethanol are quite
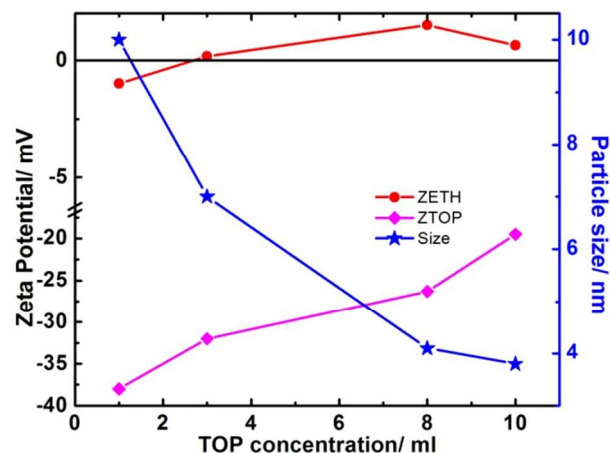

Fig. 4 Zeta potential in ethanol (ZETH) and trioctylphosphine (ZTOP) for various TOP concentrations. Different dispersants were used to see their influence on zeta potential considering the media within which samples were prepared or treated later after preparation as that might influence the nanolattice. Right axis shows the particle size variation with TOP concentrations that show increase in particle size (Size curve) as the concentration (in ml) of the latter decreases. See text, for details.

FTIR studies

The ionic state of the nanoparticles seen from the zeta potential can further be substantiated using the FTIR spectroscopy of these samples. They are represented in Figure 5 in which the spectra for ethanol, OAm and TOP are also included for reference. These spectra indicate clearly that the TOP-cum-OAm-stabilized
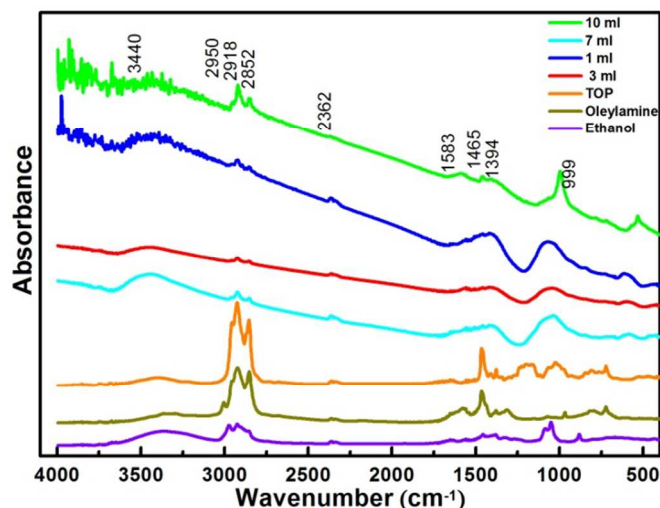

Figure 5 FTIR spectra of 1 ml, 3 ml, 7 ml and 10 ml samples along with trioctylphosphine, oleylamine and ethanol as identified in the legend.

nanoparticles resemble –in overall- a superposition of the spectra of the constituents. They reveal the C-H stretching absorption of TOP

and OAm near 2950 cm⁻¹, 2918 cm⁻¹ and 2852 cm⁻¹. The C–P and C-N stretching peaks of TOP and OAm are seen as energy band between 1217 and 910 cm⁻¹. Moreover, the absorption band between 1700 cm⁻¹ and 1300 cm⁻¹ is originated from the asymmetric in-plane and symmetric rocking mode of terminal methyl group of TOP and OAm. In addition, the peaks near 1583 cm⁻¹ and 999 cm⁻¹ have been assigned to the presence of acetylacetonate ligands.[30] This may indicate that acac ligands are attached to the phosphorus atoms of TOP to form its complex. From these data, it could be confirmed that the TOP and OAm ligands were successfully capped on the surface of the Ni nanoparticles.

XPS studies

XPS studies have been conducted on the 10 ml sample as a representative to substantiate the observations in zeta potential and FTIR data. Their spectra are shown in Figure 6. The peaks at 855.0 eV and 858.4 eV clearly indicate the presence of neutral (metallic) nickel and Ni^{2+} (Figure 6a). They suggest that nickel is partially oxidized on the surface and core nickel is metallic. The higher energy peak value at 858.4 eV than that of bulk nickel oxide (854.0 eV)[31] is understood to be due to the quantization size effect.[32] The peak at 401.2 eV (Figure 6b) indicates the presence of nitrogen due to OAm as surfactant. The presence of phosphorous due to TOP is apparent from peaks seen at 131.2 eV and 134.8 eV (Figure 6c). The peak at 131.2 eV is assigned to the substitution of P for Ni[33,34] while that at 134.8 eV to P of TOP in agreement with other reports.[34-36] The XPS peak position at 533.7 eV (Figure 6d) is identified as oxygen in acetylacetonate ligands in agreement with that of FTIR data (Figure 5) and other reports on XPS.[37] The not so clear peak, but possible, at 529.6 eV[31] due to the probable oxidation of Ni, in line with Ni^{2+} peak, appears to be because of its presumably negligible surface oxidation compared to those of dominant oxygen bonds in acetylacetonate. This data clearly proves that the nanoparticles did not get oxidized completely within 24 h as against that reported earlier [6] since such measurements were done after several weeks of the sample's preparation. The XPS peak observed at 287.1 eV (Figure 6a, inset) indicates the presence of carbon compound on the surface of the nanoparticles.
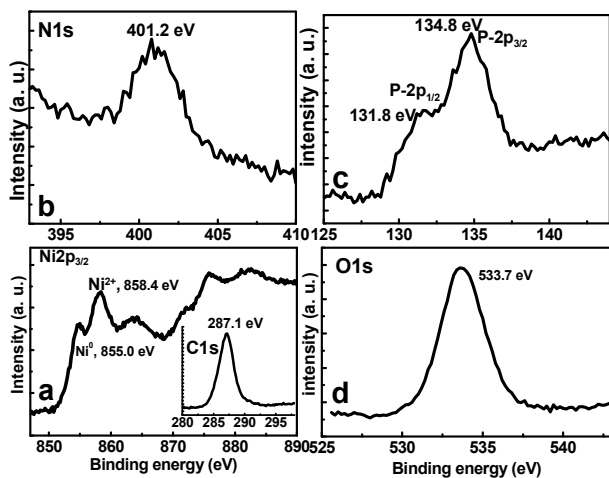

Figure 6 X-ray photoelectron spectroscopy of 10 ml nanoparticle sample. XPS spectra of (a) Ni, (b) Nitrogen, (c) phosphorous and (d) oxygen in the sample. Inset in (a): XPS spectrum of carbon.

Mechanism of the nanolattice formation

Clearly, natural nanolattice is formed when non-ionic long- and triple-chained TOP is used as surfactant, not with that of long-chain (OAm) or phenyl group (TPP) surfactant. This nanolattice formation is tentatively understood qualitatively in two ways. First, a head of surfactant (P or TOP) binds on the surface of Ni particle while organic tail in turn binds tail of another surfactant so that particles are glued at a fixed distance. When the number of such processes increases, nanolattice formation takes place with the minimization of the total surface energy. Secondly, according to zeta potential, FTIR and XPS data, cations of the ion pairs (Figure 7, inset 1') of the dissociated surfactant molecules or impurities attached on a nanoparticle may attract the anions of the surrounding nanoparticles until they sense the presence
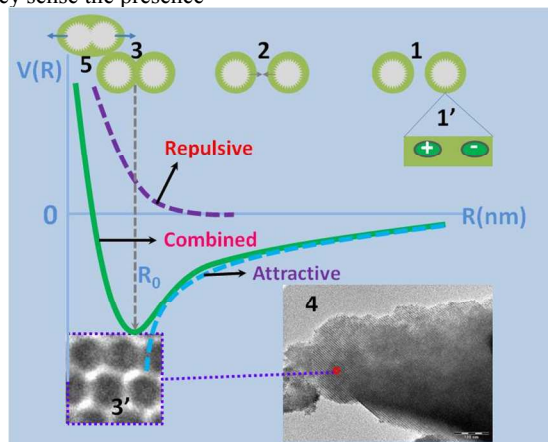

Fig. 7 Schematic plot of the proposed pair potential. The expected Coulombic nature is shown for $R > R_0$ (1,2) until it reaches an equilibrium position R_0 (3) and infinitely repulsive for $R < R_0$ (5). Each particle is surrounded by (green shell) either several surfactant molecules or ion pairs with negative and positive charges (1'). At the equilibrium position R_0 (3 or 3') nanolattice (4) is formed; scale in inset (4) is 100 nm.

of other cations of the latter leading to a repulsion. This in analogy with the electrons and nuclei of atoms in an atomic lattice[17,18] may lead to an attractive pair potential combined with repulsive potential (see also ref. [11]). This argument follows from the fact that the nanolattice formation takes place irrespective of TOP content with their c/a ratios 1.64-1.87 well-comparable to c/a ratios 1.56-1.89 of atomic lattices wherein the electrostic interaction energy of ions is so large that it completely dominates all other sources of attraction.[18] This is illustrated by nanoparticle pairs with their separation R (Figure 7). The resultant potential binds the nanoparticles enabling the observed equilibrated nanolattice (Figure 7, inset 4). The pair potential will therefore be Coulombic for $R > R_0$ until it reaches an equilibrium position R_0 (Figure 7, inset 3 or 3') and infinitely repulsive for $R < R_0$ (Figure 7, inset 5). The cohesive energy considered here is expected to include all other cohesive energies that may arise.[17,18] It may however be cautioned that it is not fully clear at this time the exact comparability of this type of bonding with that of atoms. The present results, establishing clearly the natural formation of bulk hcp nanolattices when TOP is used as surfactant and consequent resultant cohesive energy, are therefore striking. They are distinct from earlier reports that use an external energy or extra media[6-10] and show the unique property of TOP as a creator of nanolattice. The example of TOP as a former of nanolattice of at least Ni[6], ZnS and CdSe[24] clearly shows that this surfactant may be used to grow varieties of natural nanolattices of choice and the similar approach may be applied to other surfactants to enable natural nanolattice formation. Therefore, the enhanced luminescence in PbS[23] and in ZnS/ZnS and CdSe[24] is likely to be related to their nanolattices being formed.

Conclusions

In conclusion, we have successfully prepared monodispersed nickel nanoparticles of different sizes in the range of ~ 4 - 10 nm taking TOP as one of the surfactants. Such nanoparticles form outstandingly natural hexagonal close-packed nanolattices without external forces for the nanoparticles prepared as usual whenever TOP is (one of) the surfactant(s). The nanolattice parameters, calculated analytically, have c/a ratios identical to those of atomic lattices. Moreover, these results undoubtedly establish the exceptional role of nanolattice formability of TOP of several materials including, but not limited to, nickel, ZnS and CdSe. The nanolattice formability is explained based on the balanced attractive and repulsive energies of cation-anion pairs of the dissociated surfactant molecules or impurities. These findings will therefore provide a far-reaching new outlook for research in desired natural nanolattices for other similar surfactants as well, without using extra forces, and for understanding their properties for varieties of future applications.

Acknowledgements

Notes and references

[a]Department of Physics, ISLE, IPS Academy, Rajendra Nagar, Indore (MP) 452012, India.

[b]Department of Physics, Government Holkar Science College, A. B. Road, Indore (MP) 452001, India.

[c]Crystallography Laboratory, UGC-DAE Consortium for Scientific Research, Khandwa Road, Indore (MP) 452001, India.

[d]Electrical Transport Laboratory, UGC-DAE Consortium for Scientific Research, Khandwa Road, Indore (MP) 452001, India.

*Email: okram@csr.res.in, okramgs@gmail.com; Tel: +91-731-2463913, 2762267

Electronic Supplementary Information (ESI) available: [(extra XRD to compare laboratory and synchrotron results, laboratory high resolution small angle X-ray scattering data and transmission electron microscopy images]. See DOI: 10.1039/c000000x/

1 J. M. Luther, M. Law, Q. Song, C. L. Perkins, M. C. Beard and A. J. Nozik, *ACS Nano*, 2008, **2**, 271.

2 F. X. Redl, K. S. Cho, C. B. Murray and S. O'Brien, *Nature*, 2003, **423**, 968.

3 S. Sun, C. B. Murray, D. Weller, L. Folks and A. Moser, *Science*, 2000, **287**, 1989.

4 Z. Nie, A. Petukhova and E. Kumacheva, *Nature Nanotech*, 2010, **5**, 15.

5 M. P. Pileni, *J. Phys. Chem.*, 2001, **B105**, 3358.

6 J. Park, E. Kang, S. U. Son, H. M. Park, M. K. Lee, J. ; Kim, K. W. Kim, H. J. Noh, J. H. Park, C. J. Bae, J. G. Park and T. H. Park, *J. Adv. Mater*, 2005, **17**, 429.

7 D. Nykypanchuk, M. M. Maye, D. V. Lelie and O. Gang, *Nature*, 2008, **451**, 549.

8 Y. Min, M. Akbulut, K. Kristiansen, Y. Golan and J. Israelachvili, *Nature Mater*, 2008, **7**, 527.

9 K. J. M. Bishop, C. F. Wimer, S. Soh and B. A. Grzybowski, *Small*, 2009, **5**, 1600.

10 Y. Gao, Y. Bao, M. Beerman, A. Yasuhara, D. Shindo and K. Krishnan, *Appl. Phys. Lett.*, 2004, **84**, 3361.

11 E. V. Shevchenko, D. V. Talapin, N. A. Kotov, S. O'Brien and C. B. Murray, *Nature* 2006, **439**, 55.

12 X. M. Lin, H. M. Jaeger, C. M. Sorensen and K. J. Klabunde, *J. Phys. Chem.*, 2001, **105**, 3353.

13 T. Hyeon, S. S. Lee, J. Park, Y. Chung and H. B. Na, *J. Chem. Soc.*, 2001, **123**, 12798.

14 M. E. Leunissen, C. G. Christova, A. P. Hynninen, C. P. Royall, A. I. Campbell, A. Imhof, M. Dijkstra, R. V. Roij and A. V. Blaaderen, *Nature*, 2005, **437**, 235.

15 A. S. Dukhin and P. J. Goetz, surfactants in non-polar liquids, Dispersion Technology, Inc. New York 2014. http://www.dispersion.com/ionic-properti es-of-so-called-non-ionic-surfactants-in-non-polar-liquids (accessed May 20, 2014).

16 N. Bjerrum, Proceedings of the 7th International Congress of Applied Chemistry, London 1909, *Section X*, pp .55-60.

17 C. Kittel, *Solid State Physics*, 7th ed., John Wiley and Sons Inc: New York, 1996, p 55-95.

18 N. W. Ashcroft and N. D. Mermin, *Solid State Physics*, Saunders College Publishing, New York, 1976, p 395-414.

19 S. Carenco, C. Boissiere, L. Nicole, C. Sanchez, P. L. Floch andN. Mezailles, *Chem. Mater.*, 2010, **22**, 1340.

20 S. Chen, X. Zhang, Q. Zhang and W. Tan, *Nanoscale Res. Lett.*, 2009, **4**, 1159.

21 S. Sharma, N. S. Gajbhiye and R. S. Ningthoujam, *J. Colloid Interface Science*, 2010, **351**, 323.

22 N. S. Gajbhiye, S. Sharma, A. K. Nigam and R. S. Ningthoujam, *Chem. Phys. Lett.*, 2008, **466**, 181.

23 K. A. Abel, J. Shan, J. C. Boyer, F. Harris and Frank C. J. M. van Veggel, *Chem. Mater.*, 2008, **20**, 3794.

24 D. V. Talapin, A. L. Rogach, A. Kornowski, M. Haase and H. Weller, *Nano Lett.*, 2001, **4**, 207.

25 T. Mokari, M. Zhang and P. Yang, *J. Am. Chem. Soc.*, 2007, **129**, 9864.

26 B. D. Culity, *Elements of X-Ray Diffraction*, Addison-Wesley, Massachusetts, 1956.

27 A. Soni and G. S. Okram, *Appl. Phys. Lett.*, 2009, **95**, 013101.

28 G. S. Okram and Netram Kaurav, *J. Appl. Phys.*, 2011, **110**, 023713.

29 Y. Yin and A. P. Alivisatos, Nature 2005, **437**, 664.

30. http://webbook.nist.gov/cgi/cbook.cgi?ID=C3264822&Mask = 80

31. N. S. Mclntyre and M. G. Cook, *Anal. Chem.* 1975, **47,** 2208.

32 K. Borgohain, J. B. Singh, M. V. R. Rao, T. Shripathi and S. Mahamuni, *Phys. Rev. B,* 2000, **61,** 11093.

33 L. M. Moreau, D.-H. Ha, C. R. Bealing, H. Zhang, R. G. Hennig and R. D. Robinson, *Nano Lett.*, 2012, **12**, 4530.

34 M. C. Oliveira and A. M. B. do Rego, *J. Alloys and Comp.* 2006, **425,** 64.

35 J. N. Hart, P. W. Maya, N. L. Allana, K. R. Hallamb, F. Claeyssens, G. M. Fugea, M. Rudaa, P. J. Heard, *J. Solid State Chem.,* 2013, **198,** 466.

36 K. J. A. Raj, R. Sanmugam, R. Mahalakshmi and B. Vishwanathan, *Ind. J. Chem. A* 2010, **39,** 9.

37 D. Briggs and G. Beamson, *Anal. Chem.* 1993, **65,** 1517.

Table 1 Zeta potential (ζ) data with conductivity (σ) and mobility parameters (μ_H) in ethanol, hexane and TOP

Sample	Ethanol			Hexane			TOP		
(In TOP concentration)	ζ (mV)	σ (mS/cm)	μ_H (μmcm/Vs)	ζ (mV)	σ (mS/cm)	μ_H (μmcm/Vs)	ζ (mV)	σ (mS/cm)	μ_H (μmcm/Vs)
1 ml	-0.986	0.000392	-0.1768	151/125	---	0.8448	-38.0	2.78e-4	-0.01584
3 ml	0.173	0.00323	0.03098	-5.9/25	4.03e-4	-0.03307	-29.9	1.48e-4	-0.01245
8 ml	3.29	0.0102	0.5908	-102/54.7	3.82e-4	-0.5718	-26.3	1.81e-4	-0.01097
10 ml	0.639	0.00731	0.1148	6.51	6.73e-4	0.03649	-19.5	3.41e-4	-0.008115
Viscosity	0.12cP			0.2970cP			10.2cP		